The Meteoritical Society

Meteoritics & Planetary Science 45, Nr 6, 1007–1020 (2010)
doi: 10.1111/j.1945-5100.2010.01069.x

Experimental shock metamorphism of the L4 ordinary chondrite Saratov induced by spherical shock waves up to 400 GPa

Natalia S. BEZAEVA[1,2*], Dmitri D. BADJUKOV[3], Pierre ROCHETTE[1], Jérôme GATTACCECA[1], Vladimir I. TRUKHIN[2], Evgeny A. KOZLOV[4], and Minoru UEHARA[1]

[1]CEREGE, CNRS/Aix-Marseille Université, BP 80, 13545 Aix en Provence, Cedex 4, France
[2]Earth Physics Department, Faculty of Physics, M.V. Lomonosov Moscow State University, Leninskie Gory, 119991 Moscow, Russia
[3]Vernadsky Institute of Geochemistry and Analytical Chemistry, Russian Academy of Sciences, 19 Kosygin Str., 119991 Moscow, Russia
[4]Russian Federal Nuclear Center, All-Russian Research Institute for Technical Physics, Snezhinsk (Chelyabinsk-70), Chelyabinsk Region 454070, Russia
[*]Corresponding author. E-mail: bezaeva@physics.msu.ru

(Received 11 May 2009; revision accepted 07 April 2010)

Abstract–We carried out shock experiments on macroscopic spherical samples of the L4 ordinary chondrite Saratov (natural shock stages S2–S3), using explosively generated spherical shock waves with maximum peak pressures of 400 GPa and shock-induced temperatures > 800 °C (up to several thousands °C). The evolution of shock metamorphism within a radius of the spherical samples was investigated using optical and scanning electron microscopy, microprobe and magnetic analyses as well as Mössbauer spectroscopy and X-ray diffraction techniques. Petrographic analyses revealed a shock-induced formation of three different concentric petrographic zones within the shocked samples: zone of total melting (I), zone of partial melting (II), and zone of solid-state shock features (III). We found a progressive pressure-induced oxidation of Fe-Ni metal, whose degree increased with increasing shock peak pressure. The amount of FeO within zone I increased the factor of 1.4 with respect to its amount in the unshocked Saratov sample. This suggests that within zone I about 70 wt% of the initial metallic iron was oxidized, whereas magnetic analyses showed that about 10 wt% of it remained intact. This strongly supports the hypothesis that, in addition to oxidation, a migration of metallic iron from the central heavily shocked zone I toward less shocked peripheral zone took place as well (likely through shock veins where metallic droplets were observed). Magnetic analyses also showed a shock-induced transformation of tetrataenite to taenite within all shocked subsamples, resulting in magnetic softening of these subsamples (decrease in remanent coercivity). These results have important implications for extraterrestrial paleomagnetism suggesting that due to natural impact processes, the buried crustal rocks of heavily cratered solid solar system bodies can have stronger remanent magnetism than the corresponding surface rocks.

INTRODUCTION

Chondrites—primitive nondifferentiated meteorites coming from the main asteroid belt between Mars and Jupiter—form the largest group of meteorites. The main structural chondritic components are chondrules, whose origin is controversial (e.g., Hewins 1996; Zanda 2004; Lauretta et al. 2006). Chondrites and chondrules have an elemental composition similar to that of the condensable matter of the Sun and may represent the most primary source material of planetary bodies (e.g., Sears 2004; Davis 2005; Lauretta and McSween 2006). So, by investigating age, composition and texture as well as physical properties of these ancient materials we can obtain unique information on the origin and the early evolution of our solar system.

Exploration of planets, moons, and asteroids in the solar system has revealed that the majority of the solid solar system bodies (e.g., Moon, Mars, asteroids, etc.) have heavily cratered surfaces, due to an intense early bombardment by massive objects. Since the time of its formation, the solid matter of the solar system has been permanently affected by impact processes. Shock waves generated during hypervelocity impacts can deeply modify the target rock. Shock-induced changes can be observed in microstructures (Stöffler et al. 1991), texture (e.g., Schmitt 2000; Gattacceca et al. 2005) and magnetic properties (e.g., Gattacceca et al. 2007, 2008a). Thus, understanding shock phenomena in extraterrestrial materials is a key issue for deciphering physical and petrological properties of meteorites. Shock-derived changes or shock metamorphism is a common phenomenon observed in all types of meteorites (Stöffler et al. 1991; Scott et al. 1992; Nyquist et al. 2001). As the majority of shock events are characterized by both high peak pressures (up to tens or hundreds of GPa) and temperatures (thousands degrees), investigations of experimentally induced shock metamorphism in meteorites are of primary importance in planetary sciences.

Shock-recovery experiments have already been carried out on some types of chondrites (e.g., Nakamura et al. 2000; Schmitt 2000), but investigated peak pressure range remained relatively low (up to tens of GPa). The objective of this work was to investigate shock metamorphism of ordinary chondrites within a wide range of shock pressures (and temperatures) including ultra-high pressure range. For this, we conducted ultra-high pressure (up to 400 GPa) and temperature (up to several thousands °C) shock-recovery experiments on a bulk (sample A) and a powdered (sample B) macroscopic samples of the weakly shocked (natural shock stages S2–S3; Rubin 1994; Friedrich et al. 2004) non-recrystallized L4 ordinary chondrite Saratov (a fall) and carried out detailed postshock investigations of both its texture and magnetic properties.

EXPERIMENTAL SETUP AND MEASURING TECHNIQUES

All shock experiments were carried out at the All-Russian Research Institute for Technical Physics of the Russian Federal Nuclear Center (Snezhinsk, Russia).

The original material used in our shock experiments was a sample of the Saratov meteorite, provided by the Vernadsky Institute of the Russian Academy of Sciences (GEOKHI). Saratov ordinary chondrite was chosen for shock experiments due to its low level of alteration (as it is a fall, see below) and low shock stage as well as its relative accessibility (total weight of the fall: 328 kg, several stones). This meteorite is classified as an L4 ordinary chondrite (Grady 2000). The initial bulk density of the sample used for shock experiments was 3.05 g cm^{-3} (Kozlov et al. 1997). In literature, the bulk density of Saratov meteorite was found to be 2.98 ± 0.02 g cm^{-3} (Flynn et al. 1999) and its porosity, measured using He pycnometer, 13 ± 2 vol% (Flynn et al. 1999) or 15.5 vol% (Britt and Consolmagno 2003). For shock experiments, we used Saratov samples in two different forms: bulk (sample A) and powdered (sample B). Sample A was prepared in form of sphere 32 mm in diameter from the above-described bulk fragment of Saratov. For preparation of sample B, a fragment of bulk Saratov was milled into a uniform-color powder with powder fraction < 0.1 mm (the fraction size was determined by using a stainless sieve).

We conducted two technically identical shock experiments on samples A and B of Saratov. In both experiments, the corresponding sample was put into a stainless vacuum-degassed steel spherical container. The initial density of sample B was 2.43 g cm^{-3}. The assemblage was loaded with a spherically convergent shock wave according to the method described in Litvinov et al. (1991) and Kozlov and Zhukov (1994). Shock waves were generated by the detonation of a spherical layer of cyclonite-based explosive. In the B-shock experiment, the initially used powder was solidified by the shock wave propagation. During and after shock loading, the container remained hermetic and retained its strength so that the investigated meteorite matter was not contaminated by explosion products. The main advantage of the chosen shock technique (implosion using explosive) is that it allows realizing a remarkably broad range of peak shock pressures (from 25 up to > 400 GPa for the first convergent shock wave in A-experiment) and temperatures along the radii of the spherical samples (Fig. 1a).

The shock wave pattern in our samples is more complex than in plane-wave shock experiments. A shock wave converging toward the sample center progressively compresses the sample along the radius and is focused in a central region of a few mm in size (Fig. 1a). After that, a second compression wave propagates from the center outward and increases the compression state of the already shock-loaded matter (Fig. 1b). This second compression wave is accompanied by a rarefaction wave where pressure dropped. A central cavity was formed due to a radial outward flow (Figs. 2a and 2b).

The pressure-temperature profiles of the samples were calculated using the "VOLNA-81" software developed in the Russian Federal Nuclear Center

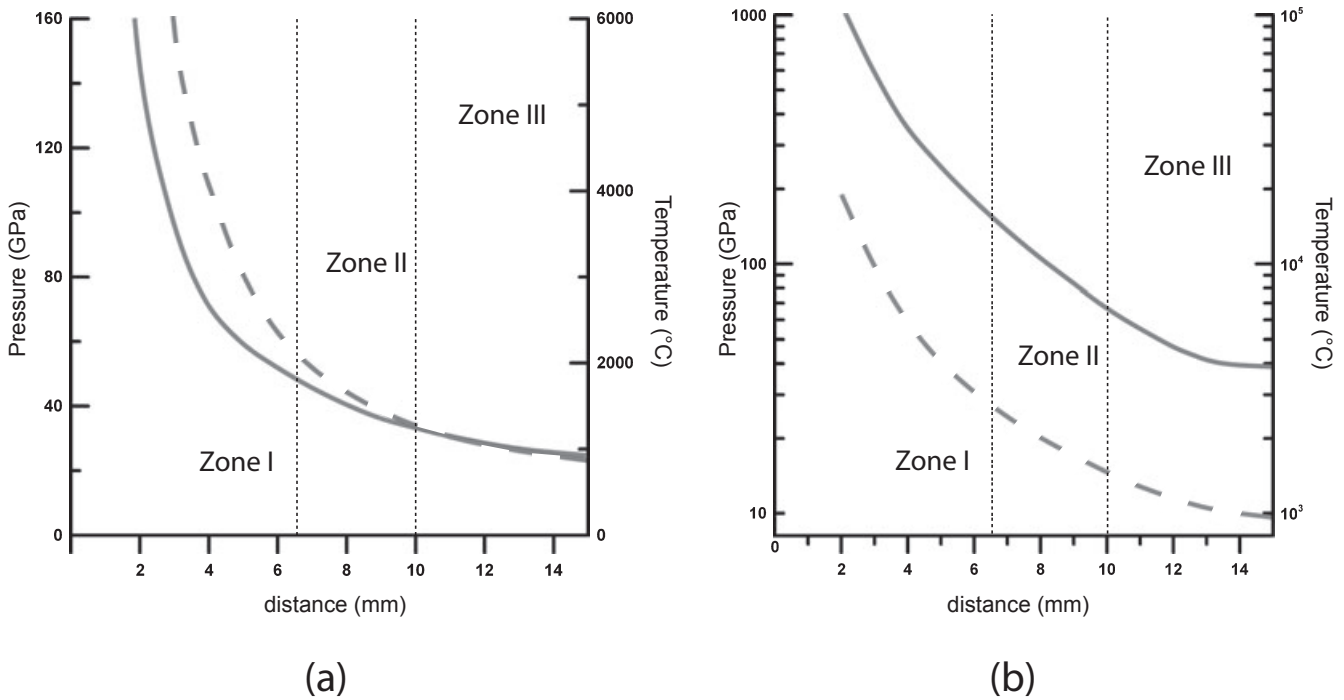

Fig. 1. Pressure and temperature profiles (solid and dashed lines, respectively) along a radius of the shocked bulk Saratov sphere (A-shock experiment). a) Calculated pressures and temperatures versus distance from the sample center corresponding to the first incoming shock wave. b) Calculated pressures and temperatures versus distance in the second compression shock wave spreading from the sphere center (reflected wave).

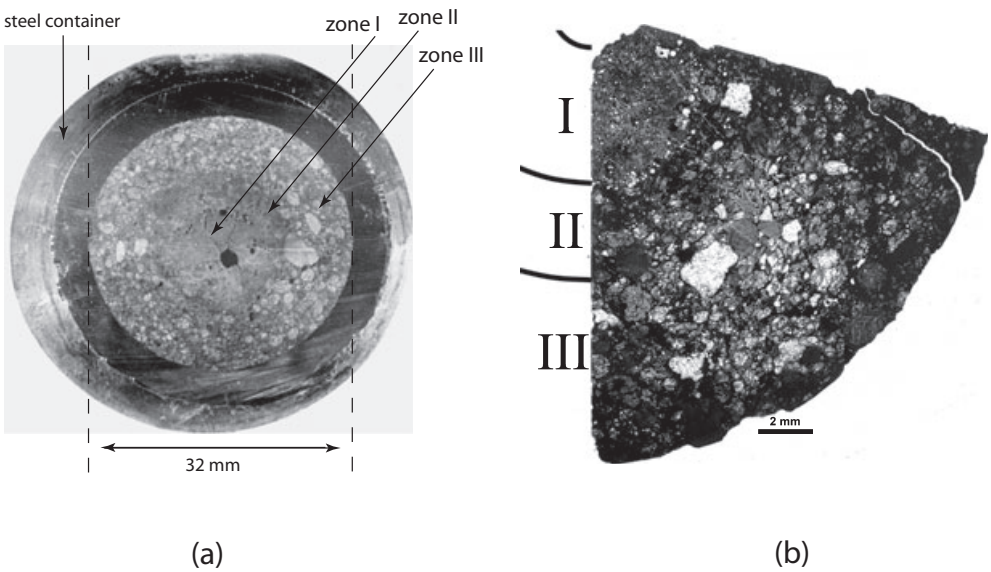

Fig. 2. Transmitted light image of a thin section from an equatorial slice of the experimentally shocked bulk Saratov spherical sample (A-shock experiment). Concentric zones of total melting (zone I), partial melting (zone II), and solid-state shock transformation (zone III) are indicated by I, II, and III, respectively. Rounded objects are chondrules, white large areas in II and III zones are holes—artifacts due to crumbling of a matter by producing the thin section.

(Snezhinsk, Russia) for numerical solving of material behavior in spherical shock waves (Kozlov and Zhukov 1994). The equation of state of the Saratov chondrite was modeled using its modal composition and equations of states of individual minerals (Ahrens and Johnson 1995). Calculated shock wave velocities (D) and particle

velocities (u) were approximated by a regression line for the initial density $\rho_{0K} = 3500$ kg m^{-3}:

$$D = 4519 + 1.369u, \quad (1)$$

where D and u are expressed in m s^{-1}. The initial porosity of 13 vol% was used in further calculations of pressure and temperature profiles. Taking into account the generalization of the used equation of state, the precision of pressure determination is ±5%. The precision of shock temperature determination is not higher than ±10% due to assumptions on the accuracy of the release adiabat path and the unknown Grüneisen parameter that was chosen to be 0.8.

In the A-shock experiment, the shock peak pressure reached 40 GPa (25 GPa in the first incoming shock wave) at the sample-container contact and rose sharply from a distance of about one-third of the sphere radius toward the center (Fig. 1a). The peak pressures in the center and at a distance of approximately 2 mm from the sample center were estimated as 400 and 153 GPa, respectively, for the first incoming shock wave and exceeded 1000 GPa for the second compression shock wave (Kozlov et al. 1997).

After unloading and cooling, shocked samples from the A and B experiments were cut along their equatorial planes to produce slices (A and B slices, respectively). Petrographic thin sections were made from sectors of the central equatorial slices A and B. We investigated the evolution of shock metamorphism along a radius of sample A thin section by optical microscopy and scanning electron microscopy. Backscattered electron (BSE) images were obtained with JEOL JSM-6400 scanning electron microscopes (SEM) equipped with energy-dispersive X-ray (EDX) analysis systems that allowed grains of different minerals to be distinguished. The BSE images were used to calculate modal compositions of experimentally shocked and unshocked samples; a modal composition of the initial Saratov sample was then recalculated to weight percents using densities of constituent minerals. Mineral phases were analyzed with the ARL-SEMQ (Naturhistorisches Museum, Vienna, Austria) and JEOL JXA-8200 electron microprobes (Oulu University, Finland) operated at a probe current of 15 nA and accelerated voltages of 15 and 25 kV for silicates and metal, respectively. Bulk chemistry was determined with a defocused 10 or 20 μm diameter beam. The microprobe was calibrated on standard oxides and silicates and the data were corrected using the ZAF correction. Detection limits are approximately 0.05 wt% for all elements. In addition to these standard analytical techniques, Mössbauer spectroscopy (Rusakov et al. 2000) and X-ray diffraction (XRD) techniques were used.

X-ray diffraction measurements were performed at CEREGE (Aix en Provence, France) on bulk a_1–a_4 samples and on a powdered subsample of initial experimentally unshocked Saratov meteorite using a PAnalytical X'Pert Pro θ/θ diffractometer with a Co Kα radiation (λ = 1.79 Å) at 40 kV and 40 mA. The 2θ range was 18–80° with a step size of 0.033° and a counting time per step of 20 s. As XRD measurements were carried out on solid samples (a_1–a_4), which, contrary to powdered samples, have preferential crystals orientation, our XRD data were only used for qualitative phase identification in shocked subsamples (only diffraction peaks location has been considered regardless of peak intensities).

Samples for the Mössbauer investigations were selected from each of the three concentric petrographic zones (see below) of both A and B shocked samples as well as from an unshocked sample of Saratov (original meteorite). Mössbauer spectra were recorded at room temperature (in absorption geometry) using a MC1101E high-speed spectrometer (Faculty of Physics, M.V. Lomonosov Moscow State University, Moscow, Russia) set in the constant acceleration mode. The used gamma source was ^{57}Co in Rh (rhodium) matrix with the activity of approximately 5 mCi. For further details, see Rusakov et al. (2000).

For magnetic investigations, we used another radial sector of the central equatorial slice A (1.5 mm in thickness) and a radial sector of the central equatorial slice B. Each sector was divided into four subsamples of approximately the same size. Subsamples from A (a_1–a_4) and B (b_1–b_4) shock experiments are numbered from the center toward periphery, respectively. Four subsamples from the B-shock experiment were only used for magnetic analyses; all petrographic and microprobe data presented below correspond to A-shock experiment (unless stated otherwise). We also used some subsamples of initial (unshocked) bulk Saratov sample (c_1–c_2). Subsamples a_1–a_4 and c_1 were also investigated using XRD technique. Here and further in the article, "shocked samples" designate experimentally shocked Saratov samples and "unshocked samples" designate initial Saratov samples, (i.e., naturally shocked to S2–S3 shock stage but unshocked experimentally in laboratory conditions). Distribution of subsamples within three identified petrographic zones (see below) was the following: subsamples a_1 and a_2 represent petrographic zones I and II, respectively, whereas subsamples a_3 and a_4 come from the petrographic zone III.

All magnetic measurements were performed at CEREGE (Aix en Provence, France). The remanent magnetization after shock and postshock saturation isothermal remanent magnetization (SIRM) of a_1–a_4

and b_1–b_4 subsamples was measured using 2G Enterprises SQUID (Superconducting Quantum Interference Device) magnetometer, equipped with online alternating field (AF) demagnetizer. This magnetometer allows a measurement of magnetic moment up to 10^{-4} Am^2 with a noise level of 10^{-11} Am^2 and AF demagnetization up to 150 mT. 3T SIRM was imparted using a pulse magnetizer MMPM9 by Magnetic Measurements. Measurements of low-field magnetic susceptibility χ_{lf} were performed with a KLY-2 Agico apparatus. Thermomagnetic heating–cooling curves between room temperature and 650 °C were measured on an unshocked sample of Saratov meteorite using MFK1-CS3 Agico apparatus. Room temperature hysteresis loops and magnetic remanence curves were obtained using a Princeton Micromag Vibrating Sample Magnetometer with maximum-applied magnetic field 1T.

Magnetic measurements on shocked Saratov samples were carried out in the following sequence. Firstly, remanent magnetization after shock experiments was demagnetized by AF up to 150 mT. After this low-field magnetic susceptibility χ_{lf}, hysteresis loops and remanence characteristics (including saturation remanent magnetization M_{rs} and coercivity of remanence B_{cr}) were measured. And finally, all samples were imparted a 3T SIRM that was measured and demagnetized by AF up to 150 mT.

To reveal shock-induced changes in remanent magnetization and intrinsic magnetic properties of experimentally shocked Saratov meteorite, we carried out the same magnetic measurements on several pieces of the initial (unshocked) Saratov meteorite (samples c_1 and c_2).

EXPERIMENTAL RESULTS

Petrography and Mineralogy

Unshocked Meteorite Sample

The initial meteorite mass was friable and consisted of easily detachable chondrules 0.1–2 mm in size and their fragments, embedded in a matrix. Outlines of the chondrules were well expressed. Chondrules displayed barred, porphyritic, and radiating textures. Our petrographic observations and electron microprobe analyses indicated that constituent phases of Saratov were: olivine ($Fa_{24–27}$, 40 wt%), monoclinic low-Ca pyroxene ($Fs_{11–21}Wo_{0.3–0.8}$, 43 wt%), high-Ca pyroxene ($Fs_{11}Wo_{35}$, 3 wt%), Fe-Ni metal (9 wt%), troilite (3 wt%), and minor minerals (apatite, chromite, shreibersite) as well as a glass partially recrystallized to feldspar–pyroxene fine-crystalline aggregates (2 wt%). Shock stage for this meteorite was determined as S2 by Rubin (1994) and as S3 by Friedrich et al. (2004) according to the shock classification of ordinary chondrites by Stöffler et al. (1991). The observed shock effects on this sample were irregular fracturing and very weak mosaicism of olivine grains. Brecciation was absent. Terrestrial alteration (occurrence of water-rich materials) in thin petrographic sections of an intact meteorite was mostly absent: it was expressed only in some areas as slight brownish coloration of silicates at the contact with metal.

Shocked Meteorite Samples

Petrographic data presented below correspond to A-shock experiment. After shock experiment, a cavity of approximately 3 mm in diameter appeared in the central part of the sample (Figs. 2a and 2b). This corresponds to the post-peak shock pressure dilatation. In the investigated thin section, three main concentric zones were observed: I—the total melt zone (1.5–6.5 mm from the center; corresponding peak pressure in the first incoming shock wave is $p > \sim$155 (50) GPa) (here and further the first pressure value designates maximum pressure in the second wave and the second pressure value between brackets designates pressure for the first incoming shock wave); II—zone of partial melting and strong shock effects in minerals (6.5–10 mm from the center; $\sim$70 (33) GPa $< p < \sim$155 (50) GPa); III—zone of the solid-state shock features in minerals (10–16 mm from the center; $\sim$40 (25) GPa $< p < \sim$70 (33) GPa) (Fig. 2).

The petrographic zones formed after shock within the bulk Saratov sample were classified according to Stöffler et al. (1991) shock stage classification for ordinary chondrites. Shock effects in zones I and II correspond to shock stages of whole rock melting (shock melted stage) and S6 (very strongly shocked), respectively. Shock effects in the inner part of zone III are the same as for stage S5 (strongly shocked), whereas the outermost part with a thickness of approximately 2 mm has shock features compatible with stage S4 (moderately shocked). Considering the two-wave structure of our shock experiment, it would not be correct to compare directly shock pressures in these zones with equilibrium peak pressures for the corresponding shock stages. However, calculations of postshock temperatures for an L chondrite (Badjukov et al. 2005) have demonstrated its total melting at 130–140 GPa that is close to a pressure value of 155 (50) GPa at a boundary between zones of total and partial melting in the Saratov sample A.

The innermost melt zone I consisted of a porous (12 vol%) quenched melt matter that was composed of olivine crystals (60 vol%) enclosed in a fine-grained mesostasis (28 vol%) of low-Ca pyroxene and glass

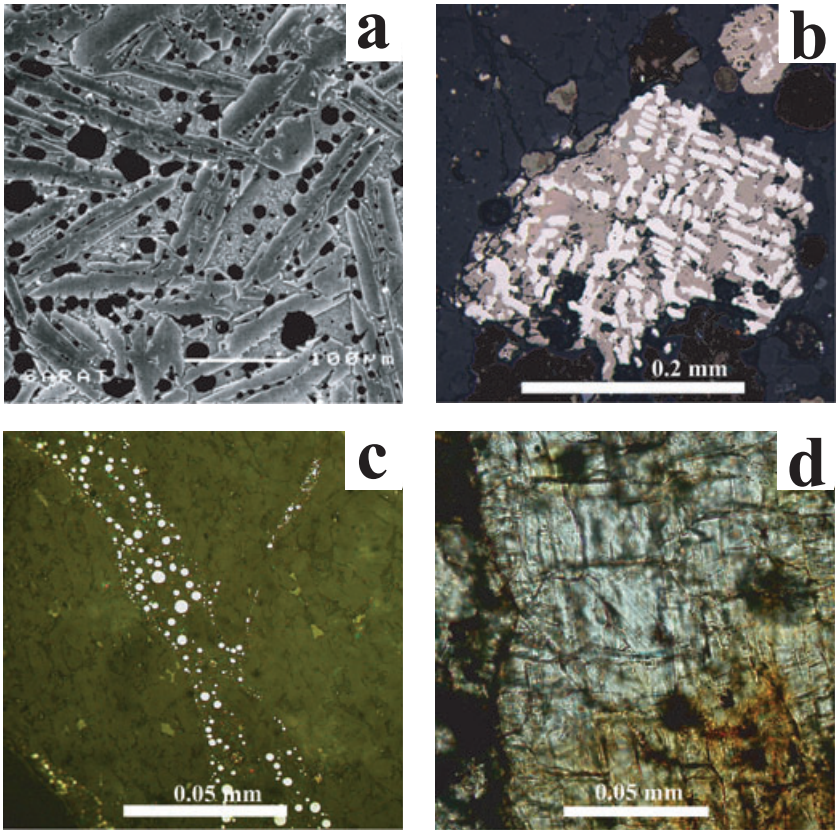

Fig. 3. Backscattered (a) and optical (b–d) microphotographs of shock effects in the bulk Saratov sample (A-shock experiment). a) Zone I: backscattered electron image showing impact melt portion consisting of bar and skeleton olivine crystals enclosed in a fine-grained mesostasis of low-Ca pyroxene and glass. b) Zone II: sulfide-metal nugget consisting of Ni-containing pyrrhotite (rose-brownish) and Ni-rich metal (white); reflected light; the distance from the sample center is 7.8 mm. c) Zone III: shock veins with metal droplets; reflected light; the distance from the sample center is 15.9 mm. d) Zone III: planar fractures and planar deformation features (fine bands of NW–SE orientations) in olivine grain; transmitted plane polarized light; the distance from the sample center is 14 mm.

(Fig. 3a). Accessories in the mesostasis were thin needles of a Ca–Cr-rich silicate and globules of an Ni-containing (up to 12 wt% Ni) sulfide(s) < 5 μm in size. The bulk silicate melt (total minus sulfides) was distinctly enriched in Fe relative to the silicate fraction of Saratov (Table 1). The composition of olivine ranged from Fa 14 (core) to Fa 40 (rim) and was rich in Cr (0.4–0.6 wt% Cr_2O_3). The mesostasis glass was rich in Si, Fe, and Ca, had an unusually high Ca/Al ratio (Table 1), and contained about 1 wt% S. Phases in the mesostasis were too small for precise analysis and identification. No Ni was detected in the silicates.

The totally melted core of the sample was surrounded by a partially melted zone II (Fig. 2). It was about 3.5 mm thick and preserved a chondritic texture. In this zone, olivines were heavily shocked and showed recrystallization, intragranular brecciation along planar fractures, brown staining and strong mosaicism with an angle of disorientation about 15–20°. The recrystallized olivines consisted of aggregates of olivine domains ranging in size from 3 to 20 μm that had or did not have similar crystallographic orientation. Angles of the disorientations vary from approximately 10° up to 120°. The recrystallized olivines were present at distances from the sample center ranging from 8.5 to 6.5 mm that corresponds to the peak pressure range from 97 (38) to 155 (50) GPa. Brown staining occured at the distances from 10.00 to 8.3 mm that corresponds to the peak pressure range from 70 (33) to 105 (40) GPa and was characterized by a uniform weak coloration of the grains. Some olivines had very low birefringence. In the inner part of this zone, there were large (up to 300 μm) sulfide nuggets associated mainly with the shock melt (Fig. 3b). They consisted of pentlandite (10–58 wt% Ni), pyrrhotite (up to 5 wt% Ni), and Ni-rich (up to 75 wt% Ni) metal. Representative analyses of the phases are given in Table 2. Some nuggets consisted of intergrowths of an iron oxide, fayalite, anorthite, and

Table 1. Chemical composition of silicate fraction (wt%) of unshocked Saratov and averages of electron microprobe data (wt%) for bulk shock melt zone I of sample A, mesostasis of the shock melt and glass in the mesostasis. All data are reduced to 100 wt%.

Analysis point	Unshocked Saratov[a]	Shock melt 29	Mesostasis 23	Glass 21
SiO_2	47.9	43.9	52.2	55.9
TiO_2	0.15	0.12	0.34	0.56
$A1_2O_3$	2.69	2.37	6.89	7.29
Cr_2O_3	0.67	0.51	0.37	0.29
FeO	14.7	20.5	26.0	17.5
MnO	0.40	0.32	0.47	0.59
MgO	29.9	28.9	3.99	1.20
CaO	2.35	2.25	6.42	13.15
Na_2O	1.01	1.00	2.92	3.24
K_2O	0.12	0.12	0.36	0.24

[a]Calculated using data of Jarosewich and Dodd (1985).

Table 2. Representative electron microprobe analyses (wt%) of metal and sulfide phases in the zone II of sample A.

	Metal	Metal	Pentlandite	Pyrrhotite
Fe	25.6	42.1	29.3	58.8
Co	0.60	1.96	0.52	0.46
Ni	73.5	55.3	37.6	4.5
S	0.22	0.56	32.5	36.1
Total	99.96	99.97	99.94	99.92

sulfide. There were also nuggets, which consisted of S-poor (0.8–7.5 wt% S; 9–20 wt% Ni) and S-rich (22–32 wt% S; 7–22 wt% Ni) metal-sulfide liquids. The S-poor liquid was always surrounded by the S-rich liquid and avoided the contact with silicates. In the outer part of the partially melted zone, there were metal and/or sulfide nuggets, which had phase composition similar to those of L chondrites. Commonly, the marginal parts of the nuggets were decorated by metal–magnetite eutectic-like intergrowths. These nuggets were enveloped by a Ni-rich (1–4 wt% Ni) magnetite. Olivine at the contact with the magnetite rim contained up to 2 wt% NiO and is rich in Fe (Fo_{65}).

The outermost zone III of the samples was a lithified zone that had a compact chondritic texture. Contrary to the sharp boundary between zones I and II, the boundary between this zone and the zone II was blurred. Boundaries between chondrules and matrix through the whole zone were sharp like in the intact meteorite. There were shock veins and melt pockets (Fig. 3c) within this zone whose occurrence rose toward the center. The veins and pockets consisted of a glass with embedded sulfide inclusions or occasionally metal droplets. Rare areas of olivine blackening were present too. The blackening was caused by intrusion of troilite into thin (< 1 μm) cracks in the grains. Planar fractures (PFs) occurred in most olivine grains and usually there were two sets of PFs although some olivine grains closer to the zone II carried up to four sets of PFs. Planar deformation features (PDF) could be observed occasionally in olivine grains and there was no more than one set of PDF per a grain (Fig. 3d). Olivine showed mosaicism whose degree developed progressively toward the zone II and a disorientation angle ranged from 2° to 3° in the outer part of the zone up to 10° in the inner part. Low-Ca clinopyroxenes were stable and did not show any shock metamorphic features except mechanical twinning along (001) plane. Unfortunately, small sizes of plagioclase grains did not allow observing the shock effects in them but it seems that they were converted to maskelynite. Metal and troilite in this zone had a normal L chondrite composition and did not show any significant oxidation. There are not any traces of a contamination or reactions between stainless container material and the sample.

X-ray diffraction measurements, carried out on macroscopic subsamples a_1–a_4 and thus more volume-representative than SEM and microprobe analyses, confirmed above-described results on the phase composition of three petrographic zones and indicated the presence of olivines within all zones and pyroxene within zone I. The presence of metallic iron or/and kamacite was shown for zones II and III only (no metal found within zone I). The possible presence of troilite within all zones and pyrrhotite within zones II and III was indicated as well.

Mössbauer spectroscopy data (Rusakov et al. 2000) demonstrated a progressive oxidation of Fe-Ni metal with increasing shock pressure toward the center. The outer zone contained Fe^{2+} in silicates and Fe^0 in metal and sulfides in proportions very close to normal L chondrite proportions. Also there was a small amount of iron in form of Fe^{3+}. The inner zones demonstrated progressive depletion of metallic iron Fe^0 by enrichment of Fe^{2+} in silicates relative to the outer zone (Fig. 4). Figure 4 (Rusakov et al. 2000) displays calculated from Mössbauer data relative Fe content within all iron-bearing mineral phases, which were fixed on Mössbauer spectra (olivine, pyroxene, wüstite, troilite/pyrrhotite, metallic iron/kamacite, and chromite/magnetite) versus distance from the spherical sample center for sample A (bulk sample).

As follows from microprobe analyses and corresponding calculations (Table 1), the amount of paramagnetic iron (FeO) within zone I (shock melt) with respect to its amount in the silicate fraction of the experimentally unshocked Saratov increased by a factor of 1.4.

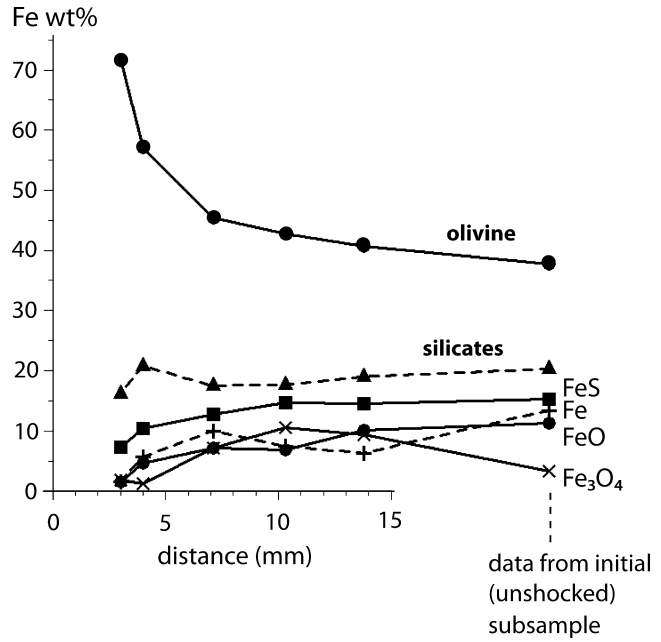

Fig. 4. Relative Fe content (all Fe is 100%) for iron-bearing mineral phases found in the shocked bulk Saratov meteorite (A-shock experiment) versus distance from the spherical sample center, calculated from Mössbauer data (Rusakov et al. 2000). The data points right from the labeled horizontal axis come from a separate unshocked Saratov sample (other than c-subsample).

After shock loading the powdered sample B had a diameter of 29 mm. Three concentric zones were observed in a thin section of sample B as well but concentric zone boundaries were shifted toward sample surface. The zone of total melting, situated in the central part of the sample, was characterized by 20% porosity and consisted of euhedral isometric and bar-like olivine crystals embedded in a mesostasis of fine-grained pyroxene and glass. At a distance of approximately 9 mm from the sample center, which corresponds to peak pressure of approximately 80 GPa, it was bordered by an approximately 2 mm thick zone of partial melting consisting of olivine and pyroxene grains in a re-melted matrix. The outermost zone was composed of chondrules, their fragments, and mineral grains cemented by a glassy mesostasis including dusty mineral clasts.

Magnetism

As mentioned above, magnetic measurements were carried out on subsamples a_1–a_4 and b_1–b_4 from A- and B-shock experiments. a_1 and a_2 represent petrographic zones I and II, respectively, whereas a_3 and a_4 come from petrographic zone III. Main magnetic properties of all subsamples (including initial fragments of Saratov meteorite c_1 and c_2) are presented in Table 3.

Magnetic minerals in L ordinary chondrites are known to be metallic Fe-Ni: kamacite (body-centered cubic with Ni ≤ 7%), taenite (face-centered cubic with Ni ≥ 7%), and more rarely tetrataenite (tetragonal $Fe_{0.5}Ni_{0.5}$). Previous petrographic studies indicated that these three forms were present in Saratov meteorite (Clarke and Scott 1980). Tetrataenite is usually characterized by a high value of magnetic coercivity B_c (~100 mT; Sugiura and Strangway 1988) whereas B_c of kamacite is known to be very low (~0.5 mT; Sugiura and Strangway 1988).

Mean magnetic coercivity for tetrataenite-rich LL chondrites (measured only on falls) is $B_c = 40.7 \pm 31.5$ mT ($n = 52$) (Gattacceca et al. 2008b) whereas for taenite and kamacite-rich H and L chondrites it is $B_c = 0.9 \pm 0.5$ mT ($n = 14$) and $B_c = 5.3 \pm 4.0$ mT ($n = 20$), respectively (Gattacceca et al. 2008b).

As seen from Table 3, low values of magnetic coercivity B_c for unshocked samples (mean $B_c = 5.4 \pm 1.5$ mT) indicated to a limited amount of tetrataenite, consistent with a chondrite of L class. Mean coercivity of shocked subsamples remained low as well (mean $B_c = 4.4 \pm 1.8$ mT). Nevertheless, the strong remanent coercivity B_{cr} of unshocked samples (from 120 to 160 mT) suggested that magnetic remanence was dominated by tetrataenite. After shock experiments B_{cr} decreased dramatically within all shocked subsamples (see Table 3, subsamples a_1–a_4; b_1–b_4 against c_1–c_2). The observed shock-induced decrease in B_{cr} was more likely caused by the conversion of tetrataenite into taenite due to the high temperature produced by shock heating. Such conversion is known to take place at heating above approximately 550 °C (e.g., Wasilewski 1982, 1988; Sugiura and Strangway 1988; Gattacceca et al. 2003). This conclusion was confirmed by an independent experiment on a nonshocked Saratov sample, heated up to 650 °C under argon atmosphere (its B_{cr} dropped from ~140 mT before heating down to ~20 mT after heating).

Formation of metal spherical droplets (observed in thin section, see Fig. 3c) by shock melting also helps to decrease coercivity with respect to initially angular grains. In both shocked bulk and powdered meteorites (from A- and B-shock experiments, respectively), subsamples from the center had on average a lower remanent coercivity than from the outer zone, highlighting the control of remanent coercivity decrease by melting. Thus, in this case, such intense shock phenomenon up to melting made ferrimagnetic grains magnetically softer contrary to the shock-induced magnetic hardening that was observed at lower

Table 3. Main magnetic properties of unshocked and shocked samples of Saratov.

Sample name	m	χ_{lf}	NRM	SIRM	M_s	B_{cr}	B_{cr}/B_c	M_{rs}/M_s
a_1	49.8	10.0	3.15	47.6	1.54	29	5.96	0.033
a_2	65.1	43.5	5.47	36.4	8.63	31	9.34	0.015
a_3	76.6	36.4	6.55	363	8.42	39	4.90	0.049
a_4	81.4	81.2	8.33	729	16.71	32	5.55	0.050
b_1	34.0	31.2	8.53	133	4.51	17	4.24	0.032
b_2	45.1	21.4	4.26	89.3	3.15	15	4.18	0.030
b_3	62.6	34.1	1.09	60.5	5.75	17	5.67	0.015
b_4	64.6	61.8	5.20	128	11.50	29	11.40	0.013
c_1	54.1	64.9	0.57	409	16.54	162	24.85	0.025
c_2	50.4	90.1	0.74	302	18.17	124	28.44	0.018

Note: m is mass (in mg). NRM and SIRM are postshock *natural remanent magnetization* and *saturation isothermal remanent magnetization* in ($\times 10^{-3}$ Am^2 kg^{-1}), respectively. χ_{lf} is low-field magnetic susceptibility in ($\times 10^{-6}$ m^3 kg^{-1}). M_s and M_{rs} are saturation magnetization and saturation remanent magnetization in Am^2 kg^{-1}. B_{cr} and B_c are magnetic coercivity and coercivity of remanence, respectively.

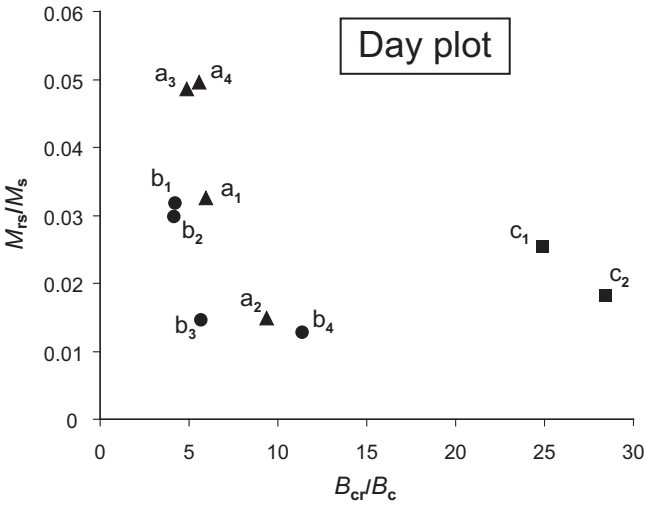

Fig. 5. M_{rs}/M_s versus B_{cr}/B_c (Day plot) for all investigated experimentally shocked (a_1–a_4; b_1–b_4) and unshocked (c_1, c_2) subsamples of Saratov meteorite. M_{rs} and M_s are saturation remanent and induced magnetizations, respectively. B_c and B_{cr} are coercivity and coercivity of remanence, correspondingly.

pressures (Gattacceca et al. 2007; Louzada et al. 2007). M_{rs}/M_s ratio versus B_{cr}/B_c (so-called Day plot) for all investigated experimentally shocked and unshocked subsamples is presented in Fig. 5. As seen from Fig. 5, all shocked samples were shifted to the left with respect to initial unshocked samples (c_1 and c_2), i.e., multidomain Fe-Ni grains became smaller. It was most likely due to shock-induced grain fragmentation. The comparison between melted and unmelted zones seems to be contradictory: the melted zone showed larger and smaller grain size for the bulk and powdered samples, respectively.

Alternating field demagnetization up to 150 mT of a_1–a_4 samples after shock indicated two-component remanent magnetization (components 1 and 2 in orthogonal projection plots, see Figs. 6a and 6b). The most relevant types of remanent magnetization that could be involved into interpretation were shock remanent magnetization (SRM), thermoremanent magnetization (TRM) or artificially induced isothermal remanent magnetization (IRM). Due to a very high minimum postshock temperature (reached in the border of the spherical sample) >800 °C, the original natural remanent magnetization (NRM) could not have survived the shock experiment. As the shock temperature peak always postdated the pressure peak, any SRM was likely to have been reset by temperature.

The REM′ method, described by Gattacceca and Rochette (2004), was used to determine the origin of both components of magnetic remanence (Fig. 7). This method is based on normalization by IRM derivative versus AF (REM′ = ΔNRM/ΔIRM) and is applicable to multicomponent magnetizations. The most resistant component of magnetic remanence (No. 1 in Figs. 6a and 6b) was characterized by a REM′≈2% so that this component may have been a TRM acquired in a magnetic field about 50 μT. Moreover, the direction of this component was the same for all samples, in agreement with a TRM acquired during cooling of the unloaded sample from the postshock temperature above Curie point down to room temperature in the Earth's magnetic field. The observed REM′ value was in agreement with experimental data on metal (Kletetschka et al. 2003), demonstrating that shock heating produces the same magnetization as room pressure heating, despite the fact that cooling occurs very rapidly (for the reversible syn-shock part) and at still high pressure. Similar REM′ values were observed in the center and periphery, suggesting that melting did not change the TRM acquisition. The low-coercivity component (No. 2 in Figs. 6a and 6b) of the post-SRM was acquired after cooling (because it is superposed to the component No. 1). So, it could not be the SRM acquired during shock experiment. Thus, this component is more likely due to some laboratory manipulations: it may correspond to an IRM acquired at exposure of the sample to an artificial magnetic field (e.g., at contact with a magnetic object). The REM′ of the low-coercivity component (up to 10%) was indeed typical of IRM (Verrier and Rochette 2002; Gattacceca and Rochette 2004). Such artificial magnetic contamination could have occurred between the time of shock experiments and the time of corresponding magnetic measurements. REM′ values of the initial (experimentally unshocked) Saratov samples

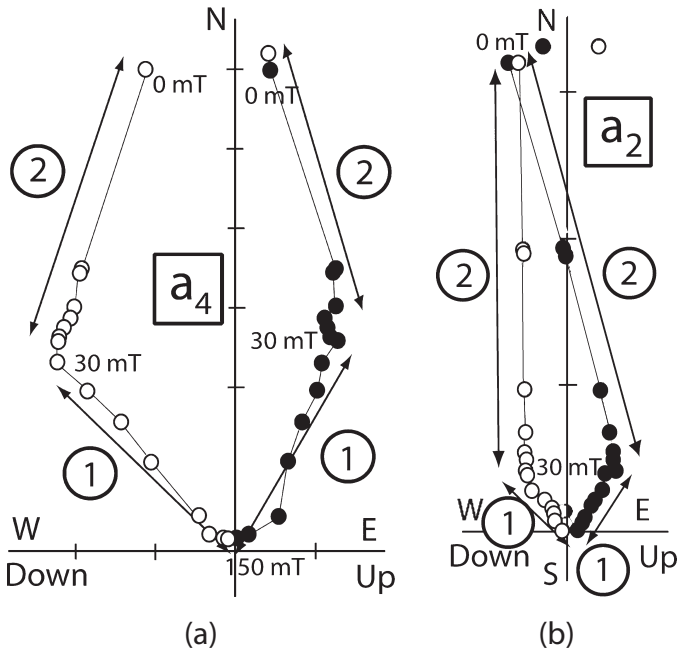

Fig. 6. Zijderveld diagrams (orthogonal projection plots) for experimentally shocked subsamples a) a_2 and b) a_4, respectively, obtained at stepwise alternating field demagnetization up to 150 mT of the residual remanent magnetization of subsamples from the bulk heavily shocked Saratov meteorite (A-shock experiment).

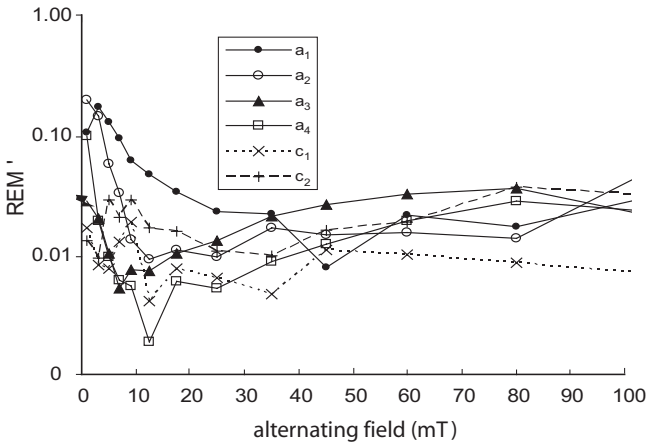

Fig. 7. REM′ (= dNRM/dSIRM) ratio versus alternating field (in mT) for experimentally shocked (a_1–a_4) and unshocked (c_2, c_3) subsamples of Saratov meteorite (A-shock experiment on the bulk Saratov sample). NRM is natural remanent magnetization and SIRM is saturation isothermal remanent magnetization.

were also high (1%). Such relatively high value for ordinary chondrite (Gattacceca and Rochette 2004) may be typical of NRM carried by tetrataenite.

Magnetic analyses allowed quantifying the amount of metallic iron Fe^0 within different petrographic zones of the bulk Saratov sample by normalizing measured M_s values of each shocked subsample (a_1–a_4) on the known M_s value of kamacite ($M_s \approx 220$ Am^2 kg^{-1}; Sugiura and Strangway 1988). This gave 0.7 wt% of metallic iron within zone I (subsample a_1), 3.9 wt% within zone II (subsample a_2), 3.8 and 7.6 wt% within zone III (subsamples a_3 and a_4, respectively). On the other hand, the estimated amount of metallic iron within the outer part of the zone III was close to its amount within initial experimentally unshocked Saratov samples: 7.5 and 8.3 wt% for subsamples c_1 and c_2, correspondingly. Thus, the amount of metallic iron within the melted heavily shocked zone (zone I) with respect of its amount in the outer part of zone III decreased by a factor of approximately 10 (for A-shock experiment).

Figures 8 and 9 display low-field magnetic susceptibility χ_{lf} and saturation magnetization M_s versus radial position of the subsample for all shocked subsamples and the initial Saratov samples. In the periphery (sample a_4), both values (χ_{lf} and M_s) correspond to those of experimentally unshocked samples. χ_{lf} and M_s have lower values toward the center of the shocked spherical sample (showing progressive decrease from a_4 to a_1 samples) indicating either the oxidation of metallic iron into paramagnetic phases (likely Fe^{2+} in silicates) or/and the segregation of metallic droplets that would have migrated toward the lower pressure zone (along pressure gradient). χ_{lf} and M_s values for the a_4 subsample and experimentally

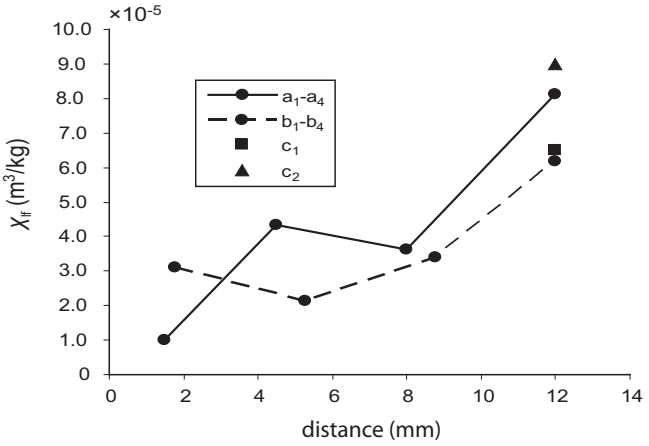

Fig. 8. Low-field magnetic susceptibility χ_{lf} for subsamples of experimentally shocked Saratov meteorite (subsamples a_1–a_4 correspond to A-shock experiment on a bulk Saratov sample and b_1–b_4 correspond to B-shock experiment on a powdered Saratov sample) versus its distance from the center of the corresponding shocked spherical sample (every point corresponds approximately to the subsample center). χ_{lf} values of the initial (experimentally unshocked) Saratov subsamples c_1 and c_2 are indicated by a square and a triangle.

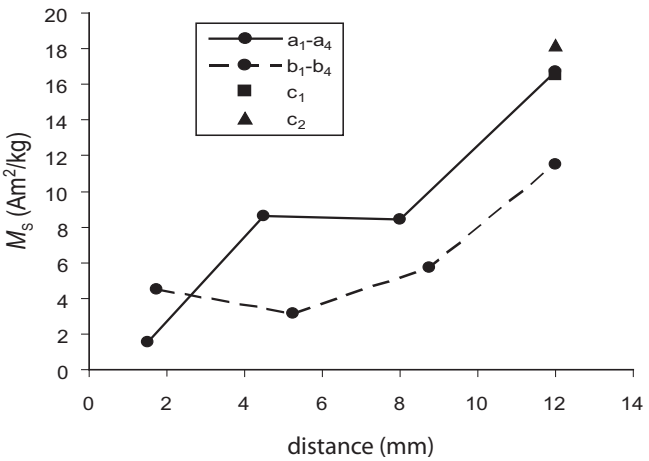

Fig. 9. Saturation magnetization M_s for subsamples of experimentally shocked Saratov meteorite (subsamples a_1–a_4 correspond to A-shock experiment on a bulk Saratov sample and b_1–b_4 correspond to B-shock experiment on a powdered Saratov sample) versus its distance from the center of the corresponding shocked spherical sample (every point corresponds approximately to the subsample center). M_s values of the initial (experimentally unshocked) Saratov subsamples c_1 and c_2 are indicated by a square and a triangle.

unshocked samples are very close (see Figs. 8 and 9; Table 3).

Metal oxidation may also have formed iron oxides and sulfides, which were observed in thin sections and whose presence was indicated by XRD and microprobe analyses. However, if magnetite (Fe_3O_4) or/and pyrrhotite ($Fe_{1-x}S$) have been formed, their contribution to magnetic properties is negligible, as shown by the lack of magnetite and pyrrhotite Curie-points (580 and 320 °C, respectively) on the thermomagnetic heating curves (Fig. 10). The presence of a minor Curie point in that range on the cooling curve may be indicative of magnetite formation during the heating-cooling experiment.

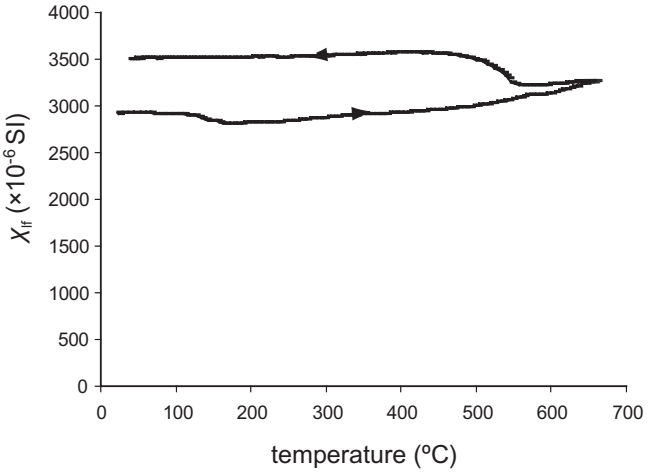

Fig. 10. Low-field magnetic susceptibility χ_{lf} versus temperature up to 650 °C for initial (unshocked) Saratov meteorite. Lower and upper curves are heating and cooling curves, respectively. Thermomagnetic heating–cooling curves were measured under argon atmosphere.

DISCUSSION

All solid-state shock features observed in the bulk Saratov sample, such as PFs, PDFs, mosaicism, etc., have been observed before, e.g., on the experimentally shocked Kernové (H6) samples (Schmitt 2000). However, melting phenomena such as shock veins and pockets, as well as total melting, have not been reproduced in the experiments on Kernové.

Also, contrary to the observation of shock-induced metallic iron nanoparticles in highly shocked Martian olivines (Van de Moortèle et al. 2007), our shock experiments show a progressive shock-induced decrease in the amount of metallic iron with increasing shock pressure toward the center of the spherical sample (in both A- and B-experiments on a bulk and a powdered Saratov samples, respectively). Optical and scanning electron microscopy observations, microprobe analyses and Mössbauer spectroscopy data, as well as magnetic data, showed a shock-induced metallic iron oxidation, whose degree increased with increasing shock peak pressure. To the knowledge of the authors, this

phenomenon has not been observed in shock experiments before.

Microprobe analyses (Table 1) indicated that the amount of paramagnetic iron (FeO) in the melted heavily shocked area (zone I) with respect to its amount in the initial (experimentally unshocked) samples increased by a factor of 1.4 suggesting that approximately 70 wt% of the initial metallic iron was oxidized and dissolved in the shock melt (as calculated from mass balance equation). Olivine compositions indicated that the melt had already been FeO-rich before olivine began to crystallize. This implies that the melt solidified before the pressure dropped to atmospheric conditions and that the oxidation was caused by the high pressure. Thus, our experiments support the possibility of high pressure metal–silicate reactions proposed earlier (Badjukov et al. 1995):

$$4Fe^{0}_{metal} + [SiO_4]^{IV}_{silicate} = 4FeO + Si. \quad (2)$$

However, contrary to data given by Badjukov et al. (1995), no reduction of Si or other elements was detected in the experimentally shocked Saratov samples with respect to unshocked samples.

Further magnetic analyses, more representative of the sample volume than microprobe analyses, showed that the amount of metallic iron within zone I with respect to its amount in the outer part of zone III (and within initial samples) decreased by a factor of approximately 10 indicating that only 10 wt% of the initial metallic iron within zone I remained intact after shock experiments. As (in zone I) 70 wt% of the initial metallic iron was oxidized and 10 wt% remained intact, this strongly supports the hypothesis of the segregation and migration of approximately 20 wt% of the initial metallic iron in form of droplets along pressure gradient from the central heavily shocked zone (I) toward lower pressure peripheral zones. Such migration could occur toward the unmelted zone III through shock veins (metallic droplets in shock veins were observed in thin section, Fig. 3c). The abundance of metallic iron in the initial (experimentally unshocked) Saratov sample was 8.3 wt% (average value). Thus, approximately 1.66 wt% of the total metallic iron has most probably migrated from zone I toward zones II and III.

Magnetic analyses on the shocked macroscopic samples did not allow confirming or disproving the hypothesis of metallic iron droplets migration as the volume ratio of the zone I with respect to zone II + zone III is extremely low (~0.07). This implies that a possible remobilization of approximately 7 wt% of metallic iron from the zone I toward periphery would result in only approximately 0.5 wt% increase in the amount of metallic iron within zones II and III. A difference < 1 wt% in the amount of metallic iron within any subsamples of Saratov meteorite corresponds to the limit of homogeneity of the initial meteoritic material and therefore can not be detected.

Thus, the decrease by a factor of 10 in the amount of metallic iron within heavily shocked zone I was likely due to both oxidation processes and migration of metallic droplets from zone I toward lower pressure zones.

Chemical nature of the oxidation (oxidation agent) was not determined exactly. We suppose that the absorbed terrestrial water could be an oxidation agent. Saratov meteorite contains 0.36 wt% H_2O (Jarosewich and Dodd 1985). One can calculate that according to the following reaction:

$$Fe^0 + H_2O = FeO + H_2 \quad (3).$$

H_2O concentration in the meteorite has to be about 1.8 wt% taking into account an oxidation of 70 wt% of metallic iron. This water content seems quite high. However, as it was shown by Badjukov et al. (2000), a converging spherical shock wave was able to provoke a shock-induced diffusion of Ar in an obsidian glass accompanied by mass-fractionation that caused an enrichment of the sample central part in Ar. The same mechanism of volatile concentration in Saratov sample center might be responsible for relatively high water concentration within zone I of the Saratov sample as the total water amount contained in the whole sample was enough to produce the observed enrichment of the melted zone in FeO. The porosity of zone I can be connected with degassing of melt during its solidification.

CONCLUSIONS

We conducted ultra-high pressure and temperature shock experiments on a bulk (experiment A) and a powdered (experiment B) macroscopic spherical samples of the L4 ordinary chondrite Saratov (shock stages S2–S3) using explosively generated spherically convergent shock waves. The used shock wave generation technique allowed realizing a wide range of peak shock pressures (from 25 GPa up to approximately 400 GPa for the first incoming shock wave) and temperatures (from 800 °C up to several thousands °C) along the radius of the spherical sample (A-shock experiment). Investigations of the corresponding thin section pointed out the formation of three different concentric petrographic zones within the shocked sample: (I) total melt zone, (II) zone of partial melting, and (III) lithified zone of the solid-state shock features.

We found that the amount of metal decreased progressively with increasing shock pressure toward the center of the spherical sample. Microprobe analyses and

Mössbauer spectroscopy data indicated that the central heavily shocked zone (I) was enriched in FeO (40 wt% increase with respect to initial experimentally unshocked samples) suggesting that about 70 wt% of metallic iron was oxidized within zone I. Oxidation agent was not determined exactly. We suppose that it could be absorbed terrestrial water. Magnetic analyses, more representative of sample volume than microprobe analyses, indicated that within zone I about 10 wt% of the initial metallic iron remained intact. This supports the hypothesis that in addition to oxidation processes, segregation and migration of 20 wt% of initial metallic iron in form of droplets from the heavily shocked zone I toward lower pressure peripheral zones took place as well most likely through shock veins as metallic droplets in shock veins were observed in thin sections.

As demonstrated by this study, the possibility for ordinary chondrites to observe shock-induced metal oxidation and remobilization of metallic droplets along pressure gradient has important implications for extraterrestrial paleomagnetism. This suggests that due to natural impact processes, on surfaces of heavily cratered asteroids, buried rocks can be more strongly magnetized compared to surface rocks. Moreover, ultra-high pressure shock events can cause mineralogical transformation of tetrataenite to taenite and thus magnetic softening (decrease in coercivity of remanence B_{cr}) of tetrataenite-bearing target rocks as well a decrease in the metal grain size.

Acknowledgments—This work was partially funded by the CNRS-RFFI PICS program (Grant No. 07-05-92165) while the stays of N. S. Bezaeva at CEREGE (Aix en Provence, France) were funded by a research grant of the French Government (bourse de thèse en cotutelle franco-russe du CROUS No. 2005814). D. D. Badjukov was supported by the Austrian Academy of Sciences and the Finnish Academy of Sciences. We thank Dr. R. T. Schmitt, the anonymous referee, and the associate editor Dr. Christian Koeberl for their numerous constructive comments and suggestions that helped us to improve our manuscript. We are grateful to Dr. F. Brandstätter from Naturhistorisches Museum (Vienna, Austria) for his help with electron microprobe, and to Dr. D. Borschneck from CEREGE (Aix en Provence, France) for his help with X-ray diffraction experiments.

Editorial Handling—Dr. Christian Koeberl

REFERENCES

Ahrens T. J. and Johnson M. L. 1995. Shock wave data for minerals. In *Mineral physics and crystallography: A handbook of physical constants*, edited by Ahrens T. J. Washington, D.C.: American Geophysical Union. pp. 143–184.

Badjukov D. D., Petrova T. L., and Pershin S. V. 1995. Impact-induced redox reactions of silicates with metal iron (abstract). 26th Lunar and Planetary Science Conference. pp. 65–66.

Badjukov D. D., Kozlov E. A., Kolesnikov E. M., Lebedeva L. M., and Nazarov M. A. 2000. Behavior of ^{40}Ar in obsidian subjected to strong shock-wave compression. *Doklady RAS, Earth Sciences* 373:905–990. In Russian.

Badjukov D. D., Brandstätter F., Kurat G., Libowitzky E., and Raitala J. 2005. Ringwoodite-olivine assemblages in Dhofar 922 L6 melt veins (abstract #1684). 36th Lunar and Planetary Science Conference. CD-ROM.

Britt D. T. and Consolmagno G. J. 2003. Stony meteorite porosities and densities: A review of the data through 2001. *Meteoritics & Planetary Science* 38:1161–1180.

Clarke R. S. and Scott E. R. D. 1980. Tetrataenite-ordered FeNi, a new mineral in meteorites. *American Mineralogist* 65:624–630.

Davis A. M., ed. 2005. *Meteorites, comets and planets*. Treatise on Geochemistry, vol. 1. Oxford: Elsevier-Pergamon. 756 p.

Flynn G. J., Moore L. B., and Klock W. 1999. Density and porosity of stone meteorites: Implications for the density, porosity, cratering, and collisional disruption of asteroids. *Icarus* 142:97–105.

Friedrich J. M., Bridges J. C., Wang M.-S., and Lipschutz M. E. 2004. Chemical studies of L chondrites. VI: Variations with petrographic type and shock-loading among equilibrated falls. *Geochimica et Cosmochimica Acta* 68:2889–2904.

Gattacceca J. and Rochette P. 2004. Toward a robust relative paleointensity estimate in meteorites. *Earth and Planetary Science Letters* 227:377–393.

Gattacceca J., Rochette P., and Bourot-Denise M. 2003. Magnetic properties of a freshly fallen LL ordinary chondrite: The Bensour meteorite. *Physics of the Earth and Planetary Interiors* 140:343–358.

Gattacceca J., Rochette P., Denise M., Consolmagno G., and Folco L. 2005. An impact origin for the foliation of chondrites. *Earth and Planetary Science Letters* 234:351–368.

Gattacceca J., Lamali A., Rochette P., Boustie M., and Berthe L. 2007. The effect of explosive-driven shocks on the natural remanent magnetization and the magnetic properties of rocks. *Physics of the Earth and Planetary Interiors* 162:85–98.

Gattacceca J., Berthe L., Boustie M., Vadeboin F., Rochette P., and De Resseguier T. 2008a. On the efficiency of shock magnetization processes. *Physics of the Earth and Planetary Interiors* 166:1–10.

Gattacceca J., Rochette P., Gounelle M., and Van Ginneken M. 2008b. Magnetic anisotropy of HED and Martian meteorites and implications for the crust of Vesta and Mars. *Physics of the Earth and Planetary Interiors* 270:280–289.

Grady M. M. 2000. *Catalogue of meteorites*, 5th ed. Cambridge: Cambridge University Press. 689 p.

Hewins R. H. 1996. Chondrules and the protoplanetary disk: An overview. In *Chondrules and the protoplanetary disk*, edited by Hewins R. H., Jones R. H., and Scott E. R. D. Cambridge: Cambridge University Press. pp. 3–9.

Jarosewich E. and Dodd R. T. 1985. Chemical variations among L-chondrites. IV. Analyses, with petrographic

notes, of 13 L-group and 3 LL-group chondrites. *Meteoritics* 20:23–36.

Kletetschka G., Kohout T., and Wasilewski P. J. 2003. Magnetic remanence in the Murchison meteorite. *Meteoritics & Planetary Science* 38:399–405.

Kozlov E. A. and Zhukov A. V. 1994. Phase transitions in spherical shock waves. In *High pressure science and technology*, edited by Schmidt S. C., Shaner J. W., Samara G. A., and Ross M. New York: American Institute of Physics. pp. 977–980.

Kozlov E. A., Zhugin Y. N., Litvinov B. V., Kovalenko G. V., Nazarov M. A., and Badjukov D. D. 1997. Features of physicochemical transformations of the Saratov chondrite at spherical shock waves. *Dokladi Akademii Nauk* 353:183–186. In Russian.

Lauretta D. S. and McSween H. Y. Jr., eds. 2006. *Meteorites and the early solar system II*, 1st ed. Tucson, AZ: The University of Arizona Press. 943 p.

Lauretta D. S., Nagahara H., and Alexander C. M. 2006. Petrology and origin of ferromagnesian silicate chondrules. In *Meteorites and the early solar system II*, 2nd ed., edited by Lauretta D. S. and McSween H. Y. Jr. Tucson, AZ: The University of Arizona Press. pp. 431–459.

Litvinov B. V., Kozlov E. A., Zhugin Y. N., Korepanov Y. M., Abakshin E. V., Kabin I. G., Simonenko V. A., Petrovtcev A. V., Kuropatenko V. F., Kovalenko G. V., and Sapojnikova G. N. 1991. On new experimental possibilities for investigations of polymorphous and phase transformations in solid-phase chemical reactions in rocks and minerals. *Dokladi Akademii Nauk USSR* 319:1428–1429 (in Russian).

Louzada K. L., Stewart S. T., and Weiss B. P. 2007. Effect of shock on the magnetic properties of pyrrhotite, the Martian crust and meteorites. *Geophysical Research Letters* 34:L05204, doi:10.1029/2006GL027685.

Nakamura T., Tomeoka K., Takaoka N., Sekine T., and Takeda H. 2000. Impact-induced textural changes of CV carbonaceous chondrites: Experimental reproduction. *Icarus* 146:289–300.

Nyquist L. E., Bogard D. D., Shih C. Y., Greshake A., Stöffler D., and Eugster O. 2001. Ages and geologic histories of Martian meteorites. *Space Science Reviews* 96:105–164.

Rubin A. E. 1994. Metallic copper in ordinary chondrites. *Meteoritics & Planetary Science* 29:94–98.

Rusakov V. S., Kupin Yu. G., Badyukov D. D., and Kozlov E. A. 2000. State of Fe atoms in minerals of the Saratov chondrite affected by spherical impact waves. *Geochemistry International* 38(Suppl. 3):383–389.

Schmitt R. T. 2000. Shock experiments with the H6 chondrite Kernouvé: Pressure calibration of microscopic shock effects. *Meteoritics & Planetary Science* 35:545–560.

Scott E. R. D., Keil K., and Stöffler D. 1992. Shock metamorphism of carbonaceous chondrites. *Geochimica et Cosmochimica Acta* 56:4281–4293.

Sears D. W. 2004. *The origin of chondrules and chondrites*. Cambridge: Cambridge University Press. 209 p.

Stöffler D., Keil K., and Scott E. R. D. 1991. Shock metamorphism of ordinary chondrites. *Geochimica et Cosmochimica Acta* 55:3845–3867.

Sugiura N. and Strangway D. W. 1988. Magnetic studies of meteorites. In *Meteoritics and the early solar system*, edited by Kerridge J. F. and Mathews M. S. Tucson, AZ: The University of Arizona Press. pp. 595–615.

Van de Moortèle B., Reynard B., Rochette P., Jackson M., Beck P., Gillet P., and McMillan P. F. 2007. Shock-induced metallic iron nanoparticles in olivine-rich Martian meteorites. *Earth and Planetary Science Letters* 262:37–49.

Verrier V. and Rochette P. 2002. Estimating peak currents at ground lightning impacts using remanent magnetization. *Geophysical Research Letters* 29, doi:10.1029/2002GL015207.

Wasilewski P. J. 1982. Magnetic characterization of tetrataenite and its role in the magnetization of meteorites (abstract). 13th Lunar and Planetary Science Conference. pp. 843–844.

Wasilewski P. 1988. Magnetic characterization of the new magnetic mineral tetrataenite and its contrast with isochemical taenite. *Physics of the Earth and Planetary Interiors* 52:150–158.

Zanda B. 2004. Chondrules. *Earth and Planetary Science Letters* 224:1–17.